Catalysis Letters (2022) 152:2840–2851
https://doi.org/10.1007/s10562-021-03858-4

Liquid "Syngas" Based on Supercritical Water and Graphite Oxide/TiO_2 Composite as Catalyst for CO_2 to Organic Conversion

Y. Gerasymchuk[1] · A. Wędzyńska[1] · W. Stręk[1]

Received: 30 September 2021 / Accepted: 5 November 2021 / Published online: 22 November 2021

Abstract

The conversion of carbon monoxide into organic substances is one of the top topics of modern science due to the development of industry and the climate changes caused by it on the one hand, and the possibility of obtaining an economic effect on the other, as it could allow for partial recovery of fuels. A problem in this regard has always been the low solubility of CO_2 in water, which eliminated the possibility of easy converting carbon dioxide into the liquid. The development of research on water critical states revealed the fact that water in a subcritical state has a much higher ability to dissolve gases. And this effect was used to obtain the "liquid synthesis gas" model presented in this paper. Equally important was the selection of an appropriate catalyst that would increase the efficiency of the conversion process by generating hydrogen in the system under the influence of cold plasma. In this work we present the studies of transformation of CO_2 dissolved in supercritical water using partially reduced graphite oxide—nanometric titania composite (RGO-TiO_2) as catalyst, due to the ability of RGO to generate hydrogen in the water environment (water splitting) under the influence of various physical factors, especially cold plasma. The RGO catalyst was stabilized with titanium oxide to obtain higher activity at lower RGO concentrations in the system. Therefore, research on conversions was preceded by a thorough analysis of CO_2 solubility in supercritical water, as well as an analysis of the structural, morphological, and spectroscopic properties of the catalyst.

✉ Y. Gerasymchuk
y.gerasymchuk@intibs.pl

[1] Institute of Low Temperature and Structure Research, Polish Academy of Sciences, 2 Okolna st., 50-422 Wrocław, Poland

Graphic Abstract
General scheme of cold plasma reactor.

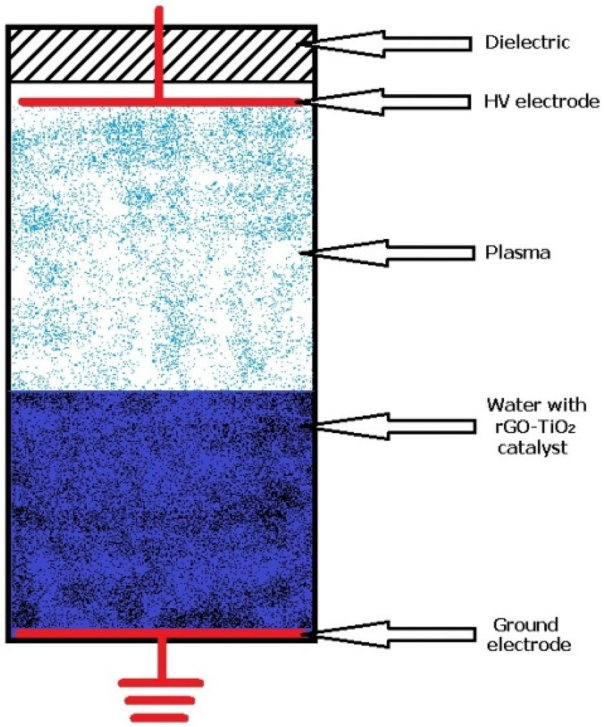

Keywords Supercritical water · Graphene-TiO_2 catalyst · CO_2 solubility · CO_2 conversion · Methanol

1 Introduction

Recently, there is observed a massive interest in studies of transformation of carbon dioxide into fuel via photocatalytic reactions. Reduction and utilization of CO_2 produced by industry is the one of most important problems of mankind. The concentration of this gas in the atmosphere increases dramatically year by year and contributes to the greenhouse effect. Such situation stimulates significantly investigations of CO_2 capture and storage in water [1–3]. It is known that the water in supercritical state allows to dissolve gases in much larger concentration [4, 5]. This supercritical state is associated with disaggregation of large waterclusters into smaller ones or even single water molecules due to the fact that hydrogen bonds are partially broken under the influence of different physical factors including high temperature and pressure in autoclaves, cold plasma, ultrasound, ionizing radiation, and laser light. The supercritical state of water is unstable in time and has a tendency to form bigger clusters, and in this stage water is also called subcritical. The supercritical water is characterized by low dielectric constant, it decreased from 78 for normal water to even 6 at the critical point [6]. In open contact with ambient atmosphere the dielectric constant quickly increases due to saturation with oxygen and nitrogen. Such state of water is called subcritical. A nature of supercritical (disaggregated) water and its role in chemical and biological systems was a subject of important studies [7, 8].

The main aim of the work was to obtain a water-CO_2 system, where the concentration of carbon dioxide would be higher than normal, with the subsequent conversion of dissolved CO_2 to organic substances under the influence of cold plasma in the presence of a catalyst which is a donor of electrons and protons (hydrogen ions). For the first time the conversion of carbon dioxide into organic compounds was described by Kolbe using the example of obtaining salicylic acid (Kolbe–Schmitt reaction) [10], so the topic itself cannot be called new. Also, there are widely used reactions of addition of CO_2 to magnesium and organolithium compounds with the formation of carboxylic acids. Our idea was to create a syngas system like that, obtained by converting of methane ($CO{\cdot}H_2O$), but in liquid form, by saturating the supercritical water with carbon dioxide. Graphite oxide for this application should be in a reduced form to eliminate the possibility of organic particles formation when it is reduced

under the influence of cold plasma, and make the experiment more accurate.

In the literature, attempts to use cold plasma in the conversion of carbon dioxide have already been reported [9–12]. Also, as it is known from the literature, a highly reduced graphite oxide (also called "flake graphene") under the influence of various physical factors, including cold plasma, is able to generate hydrogen from water [13–23]. And we use this effect in our experiment, because hydrogen interacting with carbon dioxide can lead to the formation of organic compounds, i.e. organic conversion of carbon dioxide. We decided to use a composite catalyst demonstrating a higher catalytic activity than reduced graphite oxide (RGO) [24–27]. And then, this composite, based on highly reduced graphite oxide and nanocrystalline titanium oxide in anatase form, was used as catalyst with the same cold plasma generator, that was previously used for water treatment, to convert dissolved carbon dioxide to organic compounds. We mainly meant methanol [28–30], but as a result, we also received other higher alcohols and aldehydes. After refining, this method could become the basis for developing a technological process for converting carbon dioxide into organic substances.

2 Materials and Methods

2.1 Synthesis and Properties of RGO@TiO_2 Composite

2.1.1 Obtaining of Graphite Oxide

Graphite oxide (GO) with a high level of oxidation (general formula $CO_{0.5}H_{0.2}$), as a precursor for composite, was obtained by modified Brodie method [31] from synthetic graphite (conducting grade, 200 mesh, 99.9995%, Alfa-Aesar, USA) by fourfold oxidation with potassium chlorate (99 + %, Alfa-Aesar, USA) in fumed nitric acid (98–100%, Merck, USA), and with washing with 1 M hydrochloric acid (Avantor, Poland) and distilled and deionized water until the filtrate has a neutral pH, and finally dried in a laboratory dryer with forced air circulation [32–35]. The graphite oxide obtained is a light beige powder. The high oxidation level of graphite oxide caused the high catalytic activity of obtained material due to the small linear dimensions and high degree of delamination of the material during reduction, which creates a very extensive specific surface, which is very important when using this material as a catalyst. The structure and morphology of obtained graphite oxide were confirmed by scanning electron microscopy (FESEM, FEI Nova NanoSEM 230 with EDS detector) with EDX analysis, powder X-ray diffraction pattern (PANalytical X'Pert Pro diffractometer) and Raman spectroscopy (Raman microscope inVia by Renishaw, supported with CCD camera as a detector, and laser lines 488 nm, 514 nm and 830 nm, as a source of excitation; range of measurement: 100–3200 cm^{-1}), FTIR spectroscopy (FT-IR spectrometer Biorad 575C, probes were measured in KBr pellets) and in details described in our previous works [33–35].

2.1.2 Obtaining of RGO@TiO_2 Composite Material

The target composite was obtained by the solvothermal method (GO assisted solvothermal production of TiO_2 nanoparticles) based on method described earlier by Y.L. Min et al. [36]. General procedure: 0.5 g of graphite oxide was dispersed for 30 min with (900 W 22 kHz) dispergator UZDN-M-900-T (SPE AKADEMPRYLAD Ltd, Ukraine) in 70 mL of 95% ethanol, containing 5 mL of glacial acetic acid, and then reaction mixture was cooled in an ice bath and intensively stirred on magnetic stirrer for 1 h. Afterward, 11.5 mL of titaniumbuthoxide were slowly added into above solution with vigorous stirring for 2 h. The mixture was transferred to a 100 mL stainless steel Teflon-lined autoclave, sealed and maintained at 120 °C for 24 h. During this solvothermal reaction, the GO reduced in a large degree with simultaneous deposition of TiO_2 onto the reduced graphite oxide sheets. The resulting composite was washed three times with ethanol and three times with water, then dried at 90 °C in laboratory drier with forced air flow for 72 h. Structure and morphology of obtained composite also were investigated by X-ray diffraction, FTIR spectroscopy, and scanning electron microscopy with EDX analysis, which was carried out for investigated composite in three different fields.

2.1.3 Analysis of RGO@TiO_2 Composite Surface Area

The surface area measurements of the RGO@TiO_2 composite was carried out by the method of methylene blue dye sorption on the composite surface in aqueous medium, by titration of the composite suspension in water with a dye solution followed by recording of the UV–Vis absorption spectra (BIOBASE BK-D590 double beam scanning UV/VIS spectrophotometer) according to the method described by Montes-Navajas et al. [37]. The calculation of the specific surface area is performed from the graph of the dependence of the absorption in the maximum of the methylene blue band on the concentration of the dye in the solution.

2.2 CO_2 Conversion Experiment

The supercritical water was prepared by using cold plasma technique described in our earlier works [38, 39]. Briefly, the cold plasma is produced by using nanosecond high voltage with pulsed corona discharges and acts on distilled and

demineralized water placed in a vacuum chamber (a detailed graphical diagram of the reactor is presented in the work of Psuja P et al. [39]). The voltage and the current were 2.5 kV and 30 mA, respectively. Ion flux density $R = 2.5 \times 10^6$ ions/cm^2, and the process of plasma irradiation takes usually about 1 h.

The permittivity of water was measured using Impedance Analyser HP 4191 at frequency 10 MHz and was equal to be $\epsilon = 25$, which clearly proved the supercritical feature The supercritical water is unstable and in open vessel the permittivity increases quickly in time, and after 6 h was equal to 76. The water with permittivity higher than 25 is called subcritical.

The supercritical water was saturated with CO_2 gas with laboratory carbonation system LSN2 by Sysmatec, Switzerland. Level of carbonization was estimated to be higher than 10 mg/mL.

The concentration of CO_2 was measured by analytical method (reaction of CO_2 with barium hydroxide with formation of insoluble $BaCO_3$) [40]. Barium hydroxide is very hygroscopic, so it can be anhydrous (after calcination) and can form the hydrated forms, namely: $Ba(OH)_2 \cdot H_2O$, $Ba(OH)_2 \cdot 2H_2O$, $Ba(OH)_2 \cdot 7H_2O$, and $Ba(OH)_2 \cdot 8H_2O$. For CO_2 determination, to 20.1 g of barium oxide, calcined in nitrogen flow at 400 °C (max. concentration of BaO ($Ba(OH)_2$) in water at 100 °C) in the 100 mL round bottom flask (the flask was previously dried and weighed), 20 mL of toluene and 40 mL of CO_2 saturated supercritical water were added. Toluene and water from the flask were removed by distillation under vacuum, then, the flask was heated to 400 ºC and kept at this temperature for about 2 h (also under vacuum). After self-cooling of the flask in a vacuum to room temperature, the flask was weighed again. The general reaction is as follows: $BaO + CO_2 \rightarrow BaCO_3\downarrow$.

Annealing in a nitrogen atmosphere (400 ºC) allows to completely remove the water and prevent the inclusion of CO_2 from the air. This means that the difference in the weight of the flask with BaO before reaction and $BaCO_3$ after the reaction will be the weight of the associated CO_2. The obtained amounts of $BaCO_3$ and the results of calculations of the carbon dioxide content in individual water samples, measured immediately and after 24 h, are presented in Tables 1 and 2, respectively.

Determination of the concentration of CO_2 gas was carried out using the CO2-CS Automatic CO_2 Calculating System (AT2E, France), which is used to determine the CO_2 content in beer, carbonated beverages, and sparkling wines. Measurement accuracy: ± 0.01 g/L (CO_2), ± 0.1 °C (temperature), ± 0.01 bar (pressure). 250 g of water saturated with carbon dioxide was poured into thick-walled glass bottles of 500 mL capacity (Simax, Czech Republic) and sealed with a polyethylene threaded stopper with silicone gasket. The volume of gas remaining in the bottle was 300 ± 2 mL. Partial air pressure and water compression coefficient in this case can be neglected. Five samples were prepared in this way, and they were sequentially placed in the measuring apparatus. The measurement was carried out at a temperature of 25°C. As reference, distilled and demineralized water (400 g

Table 1 Results of the chemical determination of CO_2 in fresh saturated declastered water

Water highly saturated with carbon dioxide, taken in immediately – I		
Δm ($Ba(OH)_2 \rightarrow BaCO_3$)	m(CO_2) in 1m^3 of water	Coefficient to normal quantity (1.45 kg/m^3) in room temperature
0.2862 g	7.156 kg/m^3	4.9
0.2963 g	7.406 kg/m^3	5.1
0.3373 g	8.433 kg/m^3	5.8
0.3892 g	9.731 kg/m^3	6.7
Water highly saturated with carbon dioxide, taken in immediately – II		
Δm ($Ba(OH)_2 \rightarrow BaCO_3$)	m(CO_2) in 1m^3 of water	Coefficient to normal quantity (1.45 kg/m^3) in room temperature
0.3354 g	8.385 kg/m^3	5.8
0.3768 g	9.421 kg/m^3	6.5
0.3918 g	9.795 kg/m^3	6.8
0.4399 g	10.998 kg/m^3	7.6
Water highly saturated with carbon dioxide, taken in immediately – III		
Δm ($Ba(OH)_2 \rightarrow BaCO_3$)	m(CO_2) in 1m^3 of water	Coefficient to normal quantity (1.45 kg/m^3) in room temperature
0.3271 g	8.180 kg/m^3	5.7
0.3521 g	8.800 kg/m^3	6.1
0.3841 g	9.610 kg/m^3	6.6
0.3886 g	9.715 kg/m^3	6.7

Table 2 Concentration of CO_2 in saturated subcritical water after 24 h exposition

Water highly saturated with carbon dioxide, taken after 24 h in an open vessel		
$\Delta m\ (Ba(OH)_2 \rightarrow BaCO_3)$	$m(CO_2)$ in $1m^3$ of water	Coefficient to normal quantity (1.45 kg/m^3) in room temperature
0.9277 g	5.709 kg/m^3	3.9
1.0635 g	6.545 kg/m^3	4.5
1.1503 g	7.078 kg/m^3	4.9

in a 500 mL Simax bottle) was used. Also, two Simax glass bottles were filled with the same portion of the declustered water saturated with CO_2 and left uncovered for 24 h. Then the bottles were closed and placed in a measuring apparatus.

0.5 g of RGO@TiO_2 composite material, obtained due to above method, was dispersed in 500 mL of distilled and demineralized water with high power ultrasound dispersant UZDN M900-T (22 kHz, 900 W) for obtaining the stable colloidal suspension of catalyst. Then, this suspension, placed in a special cuvette, was treated in vacuum chamber with cold plasma (description of the plasma treatment procedure is given above in Materials and Methods, Sect. 2). CO_2 was dissolved in subcritical water. After that, the water with CO_2 and RGO@TiO_2 composite was treated with plasma at room temperature by 10 min.

Chromatography measurements were performed with multifunctional gas chromatograph TSVET 800 by SPE ACADEMPRYLAD Ltd, Ukraine. The carbon dioxide content was measured in the clarified water before cold plasma treatment, and after cold plasma treatment the newly formed organic compounds were determined and their concentrations were measured.

3 Results and Discussion

3.1 Structure and Properties of Obtaining RGO@TiO_2 Composite Material

In terms of composite material obtaining, it should be noted that, unlike the method presented by Y.L. Min et al. [36], method of preparation presented here was modified in such a way that, on the one hand, it led to the formation of titanium oxide without the need for its subsequent heating in a muffle furnace. The sizes of the titanium oxide crystallites were planned to be as small as possible in the nano parameters, and as far as possible, not to gather into larger agglomerates. On the other hand, our goal was to preserve the structure of the graphite oxide so, to avoid its reduction as much as possible. The method we proposed fully met our expectations, which is confirmed by the data from the X-ray analysis. The composite material obtained in this way has a fairly developed specific surface. The performed calculations from the method of methylene blue deposition give the value of the specific surface area about 160 m^2/cm^3.

3.1.1 X-ray Diffractometry Patterns

Structure of graphite oxide precursor and obtained RGO@TiO_2 composite was examined and compared with graphite oxide and chemically reduced (with $NaBH_4$) graphite oxide (Fig. 1). When graphite oxide is reduced towards graphene structures, the characteristic reflexes at 2 theta around 12°, 26° and 42° are lost and a broad signal occurs at around 20° [41]. In a composite material, this signal is at the background level compared to the very intense reflections of the titanium oxide crystal structure in the form of anatase—JCPDS card no. 21-1272 (anatase TiO_2). The obtained results correlate very well with the data obtained for the RGO@TiO_2 composite obtained by the solvothermal (hydrothermal) method by other authors [42]. Unfortunately, the X-ray diffraction data do not allow for an accurate determination of the reduction rate of graphite oxide. It can certainly be said that it is not a fully reduced form, as there are clear reflexes in the diffractograms at 2 theta around 12° and 42°. A slight shift of the characteristic GO signal from 11.8° to 11.2° is most likely related to the formation (intercalation) of TiO_2

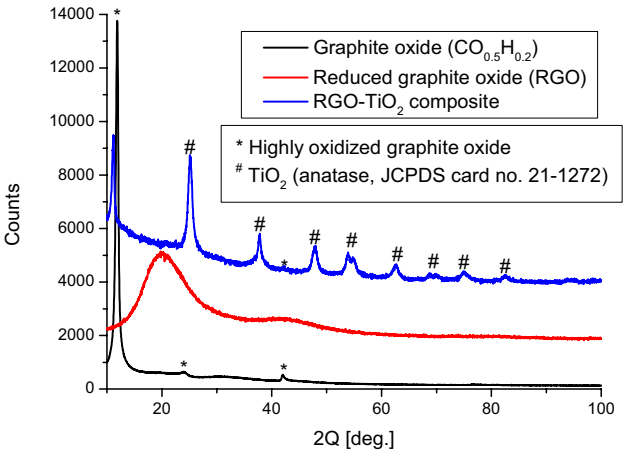

Fig. 1 XRD diffractograms of high oxidized graphite oxide (GO), chemically reduced graphite oxide (RGO) and RGO@TiO_2 composite (JCPDS card no. 21-1272 (anatase TiO_2))

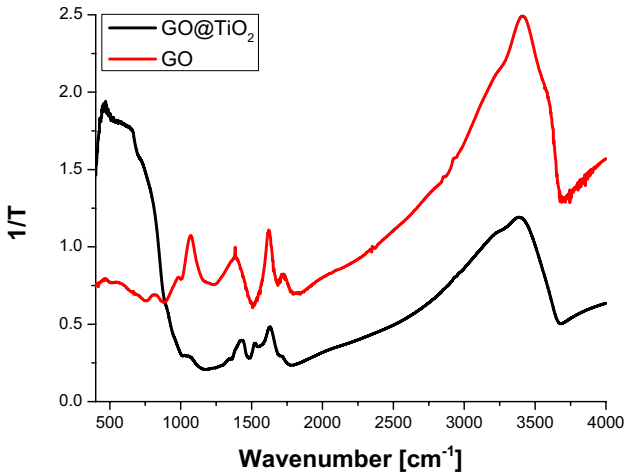

Fig. 2 FTIR spectra of obtained RGO@TiO_2 composite material recorded in KBr pellets

nanoparticles in the interplanar space of the graphite oxide layers and, accordingly, their more strong spread.

The size of the titanium oxide nanoparticles calculated from the half-width of the reflections with both, Scherer's (with Origin 2019 software) and Rietveld's (with PANalythical X'Pert HighScore Plus software) methods, was approximately 10 nm.

3.1.2 FTIR and Raman Spectroscopy

FTIR spectra of RGO@TiO_2 composite material are shown in Fig. 2, and were analyzed with ACD/Spectrus Processor software (ACD-Labs, USA) (Key: vs (very strong); s (strong); m (medium); w (weak); vw (very weak); b (broad); sh (shoulder); φ—ring; ν—stretching vibration; ρ—rocking vibration; δ—deformational or in-plane bending vibration; γ—out-of-plane vibration.) [43, 44]. The following bands at 3390 cm^{-1}(b) for RGO@TiO_2 and 3414 cm^{-1}(b) for GO (O–H) stretching vibration is prescribed to the both symmetric and asymmetric stretching vibrations of the surface hydroxyl group of titania (Ti-OH), In general, both components of composite material have broad band observed between 3600 cm^{-1} and 3000 cm^{-1}, which is related to the O-H stretching mode of hydroxyl group, indicating the presence of moisture in the sample.

Small smooth signals appeared at 2923 cm^{-1} and 2847 cm^{-1} in GO spectrum corresponded to C–H stretching vibrations. These signals indicated that the oxygen-based functional groups had been successfully grafted onto the surface and edges of the graphite sheets.

1719 cm^{-1}(w)—C = O stretching vibration from carbonyl and carboxyl groups; 1627 cm^{-1}(w)—aromatic C = C or surface absorbed water and hydroxyl groups; 1525 cm^{-1}(s)—residuals of methylene groups from titanium tetrabuthoxide; 1431 cm^{-1} (w)—residuals of carboxyl groups of GO; GO 1384 cm^{-1}(s), GO@TiO_2: 1397 cm^{-1}(sh)—O–H deformation vibration. Small signals at 1210–1235 cm^{-1}, which corresponds to C–O–C stretching of epoxy groups also are present only in GO spectrum, and signal at 1070 cm^{-1} in both spectra, corresponds with C–O stretch of the alkoxy group, were absent in composite material, but present in graphite oxide FTIR spectrum. This phenomenon is easily explained, as in the case of most composite materials with metal or metal oxide nanoparticles, these groups are the so-called centers of crystallization (especially carboxyl groups), and at the place of these groups on the surface and at the edges of the graphite oxide, nanocrystallites most often form. These groups are also reduced first under the conditions of hydrothermal synthesis.

The broad band from 1000 cm^{-1} to 400 cm^{-1} region is ascribed to the Ti-O stretching and Ti-O-Ti bridging stretching modes. For the pure TiO_2, the peaks at 464 cm^{-1} and 729 cm^{-1} in the range of 400–800 cm^{-1} are the contributions from the anatase titania. A broad absorption band between 450 cm^{-1} and 800 cm^{-1} region is ascribed to the vibration absorption of the Ti-O-Ti linkages in TiO_2 nanoparticles.

The Raman spectra of GO and RGO@TiO_2 composite were measured with 514 nm laser source and are shown in Fig. 3. Raman spectra of GO and RGO-TiO_2 samples displays two prominent peaks at 1353 cm^{-1} and 1593 cm^{-1}, which correspond to the well-documented D band and G band, respectively. A very small difference in the intensity of these bands in the composite material and in the starting GO, and especially in their relative intensity, proves that the reduction of graphite oxide is quite small. Upon reduction with hydrazine or KBH_4 (to form deep reduced form of GO) these numbers shift to lower values, 1584 cm^{-1} and 1352 cm^{-1}, with the G-band taking on a characteristic asymmetric shape. The accompanying increase in D/G ratio for RGO has been explained by the presence of smaller but more numerous sp2 domains in the carbon. Similar trends

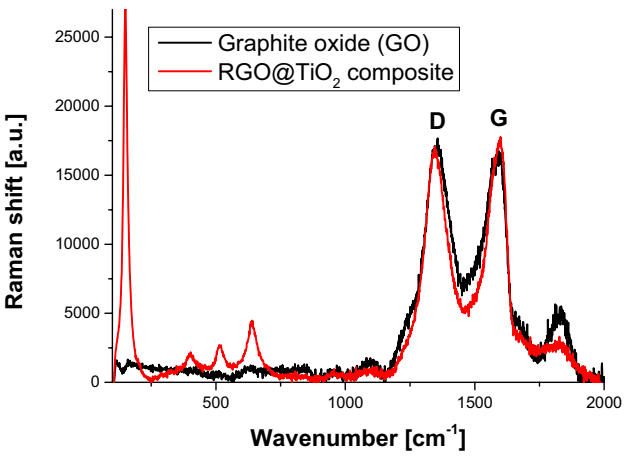

Fig. 3 Raman spectra of GO and RGO-TiO_2 samples

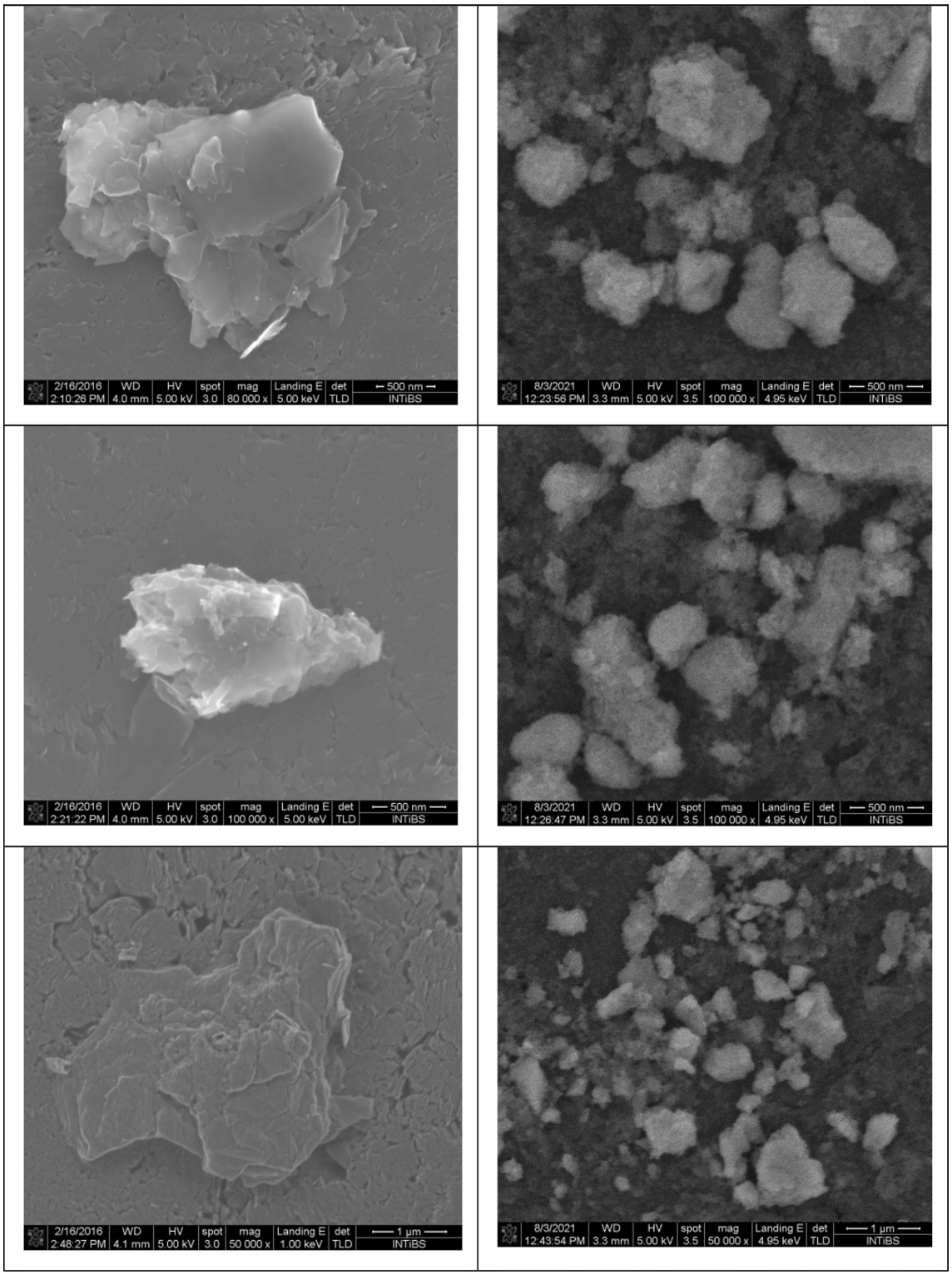

Fig. 4 SEM images of graphite oxide (left column) and RGO@TiO_2 composite material (right column) made with same resolution

are observed for very intensive peak at 144 cm^{-1} (E_g), and less intensive 396 cm^{-1} (B_{1g}), 512 cm^{-1} ($B_{1g}+A_{1g}$), and 631 cm^{-1} (E_g) indicating the presence of the anatase phase in graphene/TiO_2 composite [36, 45].

3.1.3 Morphology Measurements

As can be seen from the presented SEM images (Fig. 4), the titanium oxide particles are quite small, less than 20 nm

in size, and evenly cover stratified reduced graphite oxide plates. Moreover, the SEM images show that titanium oxide also forms larger aggregates. The results of the EDX analysis from the three measurement fields are shown in Fig. 5a–c, and the mean values are presented in Table 3. The overall average weight ratio of the components in the composite material was 88.2: 11.8, which is approximately 1:8. So, the content of TiO_2 in the composite was about 13%.

3.1.4 Determination of the Specific Surface Area in RGO-TiO_2 Composite

The graph of the dependence of the absorbance intensity in the absorption maximum of the methylene blue dye band on the dye concentration is presented in Fig. 6. As can be seen in the diagram, the surface saturation of the composite material takes place with the total addition of 45 µL of methylene blue solution, which corresponds to the amount of 0.03825 mg of the dye. The literature shows that at the maximum saturation of the surface of the tested material, the ratio of the amount of MB to the covered area is 2.54 m^2/1 mg MB. Converting this into the amount of RGO@ TiO_2 in the cuvette, we get the value of the specific surface area in the tested material of 162 m^2/g. The specific surface area of nanometric mesoporous titanium oxide in the form of anatase, which has not been calcined, according to the literature data, is below 90 m^2/g. [46–48], and the specific surface area of graphite oxide with a minimum concentration of 0.8 mg/ml is about 550 m^2/g [37]. At this point, it should be underlined, that all authors in the cited works emphasize the fact, that the specific surface of GO to a large extent depends on the concentration of the material in the tested suspension: the greater the concentration of GO in suspension, the greater was the specific surface area. In our case, the concentration was three times lower than the minimum, described in the cited works, which was related to the measuring capabilities of the spectrophotometer. At higher concentrations, the spectra were very distorted (jagged), which made their accurate interpretation impossible, and at concentrations above 0.5 mg/mL, they fell outside the absorbance measuring range (maximum absorbance value in the measuring range of the spectrophotometer was 3). Therefore, the values obtained by us are quite large, and even slightly exceed the values obtained for similar materials using the methylene blue adsorption and nitrogen adsorption with BET analysis (BET – 89 m^2/g: Huiyu Yang et al. [49]; BET – 170 m^2/g: Z. Gohari-Bajestani et al. [50]).

Table 3 Results of EDX analysis for RGO-TiO_2 composite material and calculated average values of material composition

Elements	Field 1		Field 2		Field 3		Average values	
	Wt%	At%	Wt%	At%	Wt%	At%	Wt%	At%
C	44.67	57.30	43.09	55.78	43.92	58.64	43.89	57.24
O	38.81	37.38	39.79	38.67	33.84	33.92	37.48	36.65
Ti	16.53	05.32	17.12	05.56	22.24	07.44	18.63	6.11

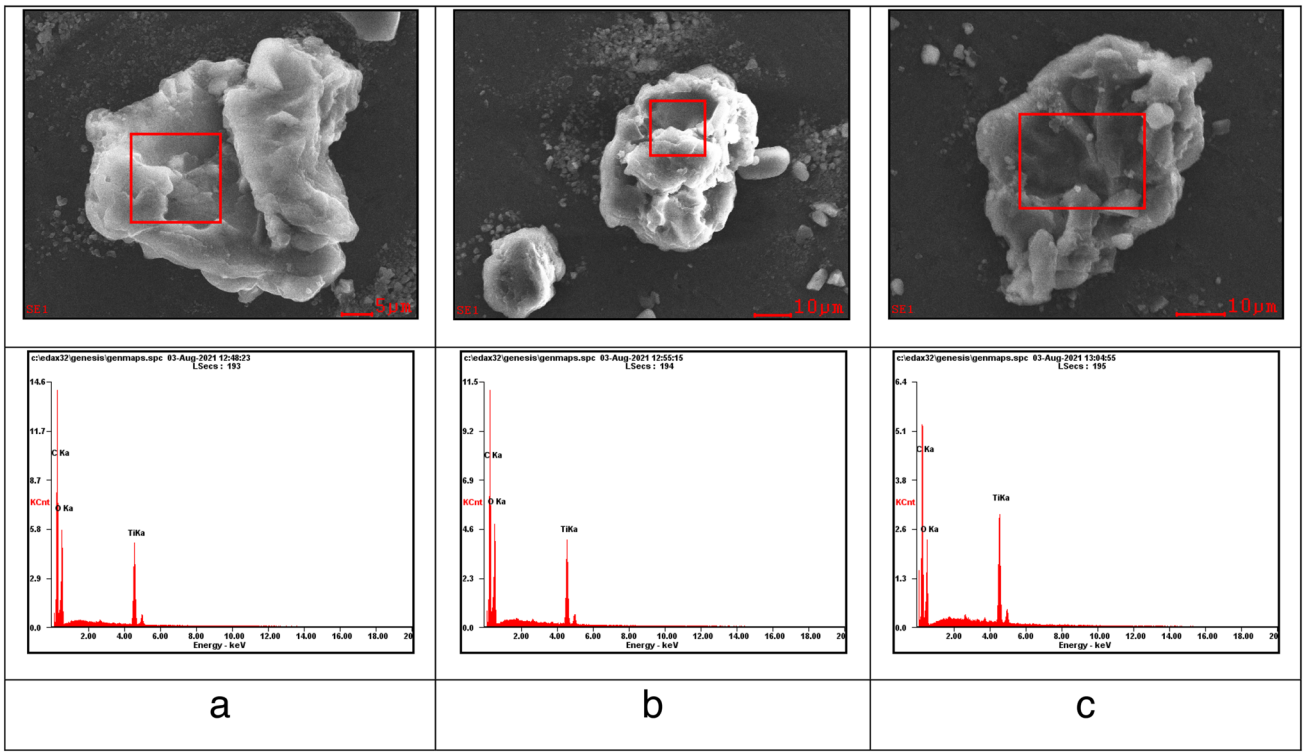

Fig. 5 EDX microanalysis reports for RGO@TiO2 composite material in three different fields of measurements

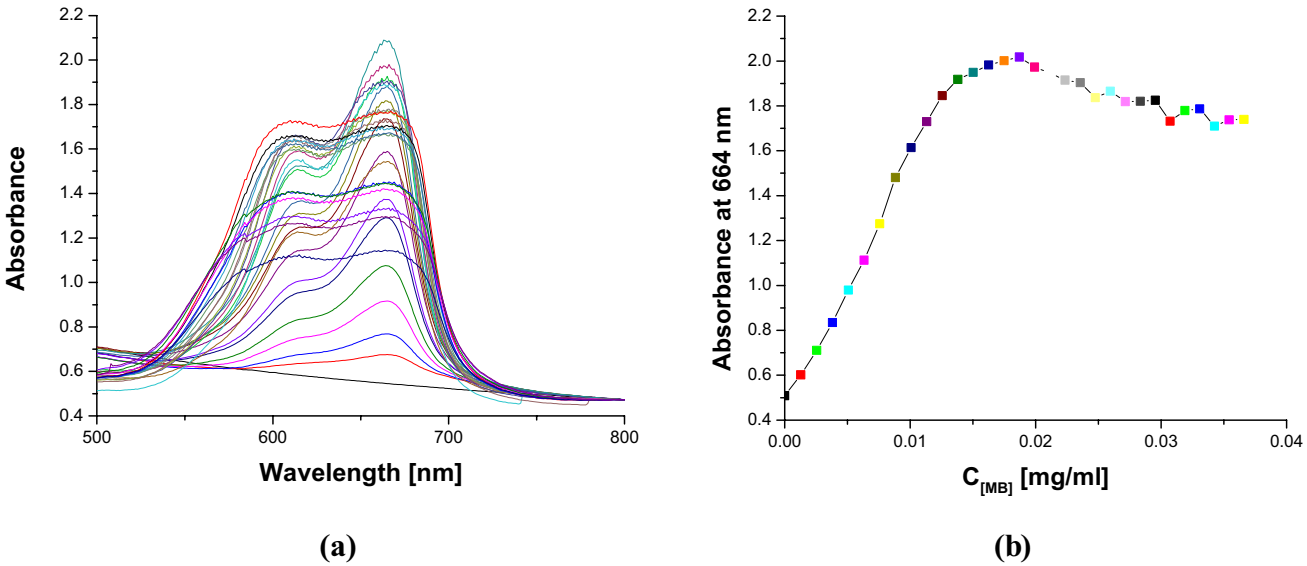

Fig. 6 Absorption spectra of methylene blue during titration of the RGO@TiO_2 composite suspension in water (**a**), and a graph of the dependence of the absorption intensity in the maximum of the methylene blue absorption band (664 nm) on its concentration in cuvette (**b**)

Table 4 Obtained parameters of the physical determination of CO_2 in fresh saturated declustered water

T [K]	$V_{(CO2)}$ [cm^3]	p_{CO2} [bar]	m [g]	c [mg/ml]
298 ± 0.1	300 ± 2	4.60	2.45	9.82
298 ± 0.1	300 ± 2	4.41	2.35	9.39
298 ± 0.1	300 ± 2	4.27	2.28	9.13
298 ± 0.1	300 ± 2	3.94	2.12	8.44
298 ± 0.1	300 ± 2	3.66	2.20	7.78

c Concentration of carbon dioxide in water [mg/ml or kg/l]

Table 5 Obtained parameters of the physical determination of CO_2 in saturated subcritical water after 24 h exposition

T [K]	$V_{(CO2)}$ [cm^3]	p_{CO2} [bar]	m [g]	c [mg/ml]
298 ± 0.1	300 ± 2	2.67	1.43	5.68
298 ± 0.1	300 ± 2	2.39	1.28	5.12

c Concentration of carbon dioxide in water [mg/ml or kg/l]

Table 6 CO_2 conversion under cold plasma treatment supported by rGO-TiO_2 catalyst

Product	Concentration in solution (mg/ml)	Percentage of conversed CO_2 (%)
Methanol	0.08	12
1-Propanol	0.02	2.5
Acetaldehyde	0.01	1.2

3.2 CO_2 Conversion Experiment

3.2.1 Determination of CO_2 Concentration in Supercritical Water

Chemical determination of carbon dioxide in water was carried out for three different supplies of water, delivered at different times. Four test samples were taken from each supply. In total, 12 samples were tested and the results are presented in Table 2. A control sample was also collected from each batch of water and left in the open flask overnight. The results of CO_2 determination for three supplies of water after 24 h are presented in Table 3. Summarizing these studies, it should be noted that the concentration of carbon dioxide ranged from 7 kg/m^3 to 11 kg/m^3, i.e. it exceeded the normal solubility of carbon dioxide in water at room temperature and normal atmospheric pressure from 5 to 7 times. After 24 h in an open flask, the concentration of carbon dioxide was slightly lower, but still remained quite high and fluctuated within 6–7 kg/m^3, i.e. 4–5 times of the norm. This demonstrates the very high content of carbon dioxide in declustered water, which opens the way for this approach to be used in industrial trapping and further conversion of CO_2.

The results of physical determination of carbon dioxide concentration in the tested samples of water are summarized in Tables 4 and 5. Table 4 presents the results of measurements of carbon dioxide concentration in water, taken immediately from pressure vessel in atmospheric pressure conditions. The results of carbon dioxide concentration measurements after 24 h of keeping water in an open thick-walled glass bottles in the air in atmospheric pressure conditions are listed in Table 5. The average values calculated from the above data for temperatures close to room temperature change from 8 mg/mL to 10 mg/mL (so respectively 8–10 kg/m^3) in water immediately after taking it from a pressure vessel, and 5–6 mg/mL (so respectively 5–6 kg/m^3) after 24 h of keeping it in an open thick-walled glass bottles at atmospheric pressure. The calculated results of physical tests correlate very closely with the data obtained by chemical analysis.

The amount of carbon dioxide needed to completely saturate 1 L of distilled water in contact with air containing 0.08–0.1 vol. % (17.1–21.4 g in m^3 of air—average content in the atmosphere 0.04%) of carbon dioxide in the room, according to global air quality standards at 760 mm Hg at room temperatures is 1.45 kg/m^3 (or 1.45 mg/mL–1.45 g/L at 25 °C, 100 kPa).

3.2.2 Conversion of CO_2 Dissolved in Supercritical Water

The results of gas chromatography measurements for cold plasma treated water with measured concentration of CO_2 = 8.25 mg/mL were presented in Table 6. The experimental results demonstrated very high efficiency of RGO@TiO_2 composite as catalyst and high potential of cold plasma treatment for synthesis of methanol. Preliminary results showed that almost 12% of CO_2 was converted into methanol. Moreover, 2.5% of CO_2 was converted to 1-propanol and 1.2% of CO_2 into acetaldehyde. The general conversion of CO_2 to organic substances at level ~ 16% in liquid phase is a very high value. These values for plasma gas systems are obviously higher—on the order of 30% [9], but in terms of obtaining liquid fuels, as shown in the literature data [12, 29], the method we have proposed is one of the most effective and may find practical application.

4 Conclusion

In the current work, a new method of conversion of CO_2 to organic molecules was presented, where a catalyst was based on a composite of graphite oxide and titanium dioxide used in supercritical water. The CO_2 concentration, that was obtained in the declustered water, was more than 10 times higher than in water under normal condition. In this system and under cold plasma treatment, the overall conversion of carbon dioxide to organics was about 16%, that was relatively high yield obtained by the optimization of presented RGO@TiO_2 catalyst. The technical parameters of the efficient capture of carbon dioxide by supercritical water, the conversion of CO_2 into organic substances, as well as a detailed analysis of the structure and properties of the used catalyst presented in this paper, may be the basis for further research on the improvement of the entire process and for the development of industrial technologies.

Acknowledgements Authors would like to thank Dr. Igor Elkin for supplying supercritical water, Dr. Maciej Ptak for FTIR and Raman measurements, and Dr. Damian Szymański for SEM and EDX measurements.

References

1. Magneschi G, Zhang T, Munson R (2017) The impact of CO_2 capture on water requirements of power plants. Energy Procedia 114:6337. https://doi.org/10.1016/j.egypro.2017.03.1770
2. Byers EA, Hall JW, Amezaga JM, O'Donnell GM, Leathard A (2016) Water and climate risks to power generation with carbon capture and storage. Environ Re Lett 11:024011. https://doi.org/10.1088/1748-9326/11/2/024011
3. Sakakura T, Choi JC, Yasuda H (2007) Transformation of carbon dioxide. Chem Rev 107:2365. https://doi.org/10.1021/cr068357u
4. Yesodharan S (2002) Supercritical water oxidation: an environmentally safe method for the disposal of organic wastes. Curr Sci 82:1112. https://doi.org/10.5772/intechopen.89591
5. Brunner G (2010) Applications of supercritical fluid. Ann Rev Chem & Biomol Engin 1:321. https://doi.org/10.1146/annurev-chembioeng-073009-101311
6. Deguchi S, Tsujii K (2007) Supercritical water: a fascinating medium for soft matter. Soft Matter 7:797. https://doi.org/10.1039/B611584E
7. Pollack GH The fourth phase of water: beyond solid, liquid, and vapor (Ebner & Sons, Seattle (USA), 2013)
8. Goncharuk VV, Science about water (Akademperiodyka, Kyiv (UA), 2014)
9. Ashford B, Tu X (2017) Non-thermal plasma technology for the conversion of CO_2. Curr Opin Green Sustain Chem 3:45. https://doi.org/10.1016/j.cogsc.2016.12.001
10. Kolbe H (1860) Ueber Synthese der Salicylsäure. Justus Liebigs Ann Chem 113:125–127. https://doi.org/10.1002/jlac.18601130120
11. Wang J, Xia G, Huang A, Suib SL, Hayashi Y, Matsumoto H (2011) CO_2 decomposition using glow discharge plasmas. Plasma Chem Plasma Process 185(1):152. https://doi.org/10.1006/jcat.1999.2499
12. Hoeben WFLM, van Hoesch EJM, Beckers FJCM, Boekhoven W (2015) Plasma driven water assisted CO_2 methanation. IEEE Transaction Plasma Sci 43(6):1954. https://doi.org/10.1109/TPS.2015.2429316
13. Min Sh, Lu G (2013) Promoted photoinduced charge separation and directional electron transfer over dispersible xanthene dyes sensitized graphene sheets for efficient solar H_2 evolution. Int J Hydrogen Energy 38:2106. https://doi.org/10.1016/j.ijhydene.2012.11.124
14. Azarang M, Sookhakian M, Aliahmad M, Dorraj M, Basirun WJ, Goh BT, Alias Y (2018) Nitrogen-doped graphene-supported zinc sulfide nanorods as efficient Pt-free for visible-light photocatalytic hydrogen production. Int J Hydrogen Energy 43:14905. https://doi.org/10.1016/j.ijhydene.2018.06.082
15. El-Maghrabi HH, Nada AA, Diab KR, Youssef AM, Hamdy A, Roualdes S, El-Wahab SA (2018) Facile fabrication of $NiTiO_3$/graphene nanocomposites for photocatalytic hydrogen generation. J Photochem Photobiolog A: Chemistry 365:86. https://doi.org/10.1016/j.jphotochem.2018.07.040
16. Min Sh, Lu G (2012) Dye-cosensitized graphene/Pt photocatalyst for high efficient visible light hydrogen evolution. Int J Hydrogen Energy 37:10564. https://doi.org/10.1016/j.ijhydene.2012.04.072
17. Tian B, Li Z, Zhen W, Lu G (2016) Uniformly sized (112) facet Co2P on graphene for highly effective photocatalytic hydrogen evolution. J Phys Chem C 120:6409. https://doi.org/10.1021/acs.jpcc.6b00680
18. Lou Z, Fujitsuka M, Majima T (2017) Two-dimensional au-nanoprism/reduced graphene oxide/Pt-nanoframe as plasmonic photocatalysts with multiplasmon modes boosting hot electron transfer for hydrogen generation. J Phys Chem Lett 8:844. https://doi.org/10.1021/acs.jpclett.6b03045
19. Fu Y, Wang G, Ming X, Liu X, Hou B, Mei T, Li J, Wang J, Wang X (2018) Oxygen plasma treated graphene aerogel as a solar absorber for rapid and efficient solar steam generation. Carbon 130:250. https://doi.org/10.1016/j.carbon.2017.12.124
20. Zhuang M, Ou X, Dou Y, Zhang L, Zhang Q, Wu R, Ding Y, Shao M, Luo Z (2016) Polymer-embedded fabrication of Co2P nanoparticles encapsulated in N, P-doped graphene for hydrogen generation. Nano Lett 16:4691. https://doi.org/10.1021/acs.nanolett.6b02203
21. Zhou Y, Zhang G, Yu M, Wang X, Lu J, Yang F (2018) Free-Standing 3D porous N-doped graphene aerogel supported platinum nanocluster for efficient hydrogen production from ammonia electrolysis. ACS Sustain Chem Eng 6:8437. https://doi.org/10.1021/acssuschemeng.8b00586
22. Shi Y, Gao W, Lu H, Huang Y, Zuo L, Fan W, Liu T (2017) Carbon-nanotube-incorporated graphene scroll-sheet conjoined aerogels for efficient hydrogen evolution reaction. ACS Sustain Chem Eng 5:6994. https://doi.org/10.1021/acssuschemeng.7b01181
23. Meng F, Li J, Cushing SK, Zhi M, Wu N (2013) Solar Hydrogen Generation by Nanoscale p-n Junction of p-type Molybdenum

Disulfide/n-type Nitrogen-Doped Reduced Graphene Oxide. J Am Chem Soc 135:10286.
24. Trzeciak AM, Wójcik P, Lisiecki R, Gerasymchuk YS, Stręk W, Legendziewicz J (2019) Palladium nanoparticles supported on graphene oxide as catalysts for the synthesis of diarylketones. Catalysts 9(4):319. https://doi.org/10.3390/catal9040319
25. Szabó T, Berkesi O, Forgó P, Josepovits K, Sanakis Y, Petridis D, Dékány I (2006) Evolution of surface functional groups in a series of progressively oxidized graphite oxides. Chem Mater 18:2740. https://doi.org/10.1021/cm060258+
26. Szabó T, Hornok V, Schoonheydt RA, Dékány I (2010) Hybrid Langmuir-Blodgett monolyers of graphite oxide nonosheets. Carbon 48:1676. https://doi.org/10.1016/j.carbon.2009.12.050
27. Szabo T, Veres A, Cho E, Khim J, Varga N, Dekany I (2013) Photocatalyst separation from aqueous dispersion using graphene oxide/TiO2 nanocomposites. Coll Surf A 433:230. https://doi.org/10.1016/j.colsurfa.2013.04.063
28. Fujishima A, Honda H (1972) Electrochemical photolysis of water at a semiconductor electrode. Nature 238:37. https://doi.org/10.1038/238037a0
29. Nazimek D, Czech B (2011) Artificial photosynthesis – CO_2 towards methanol, *E-MRS* 2010 Fall Meeting. IOP Conf Ser: Mater Sci Eng 19:01210
30. Hsu HC, Shown I, Wei HY, Chang YC, Du HY, Lin YG, Tseng CA, Wang CH, Chen LC, Lin YC, Chen KH (2013) Graphene oxide as promising photocatalyst for CO_2 to methanol conversion. Nanoscale 5:262. https://doi.org/10.1039/C2NR31718D
31. Szabó T, Tombácz E, Illés E, Dékány I (2006) Enhanced acidity and pH-dependent surface charge characterization of successively oxidized graphite oxides. Carbon 44:537. https://doi.org/10.1016/j.carbon.2005.08.005
32. Kędziora A, Gerasymchuk Y, Sroka E, Bugla-Płoskońska G, Doroszkiewicz W, Rybak Z, Hreniak D, Wiglusz R, Stręk W (2013) Use of the materials based on partially reduced graphene-oxide with silver nanoparticle as bacteriostatic and bactericidal agent. Polim Med 43:129
33. Gerasymchuk Y, Lukowiak A, Wedzynska A, Kedziora A, Bugla-Ploskonska G, Piatek D, Bachanek T, Chernii V, Tomachynski L, Strek W (2016) New photosensitive nanometric graphite oxide composites as antimicrobial material with prolonged action. J Inorg Biochem 159:142. https://doi.org/10.1016/j.jinorgbio.2016.02.019
34. Gerasymchuk Y, Tahershamsi L, Tomala R, Wedzynska A, Chernii V, Tretyakova I, Korona-Glowniak I, Rajtar B, Malm A, Piatek D, Lukowiak A (2021) Composites based on graphite oxide and zirconium phthalocyanines with aromatic amino acids as photoactive materials. Chem Pap 75(10):5421. https://doi.org/10.1007/s11696-021-01731-7
35. Gerasymchuk Y, Kędziora A, Wędzyńska A, Tahershamsi L, Chernii V, Tretyakova I, Chernii S, Pekhnyo V, Korona-Głowniak I, Malm A, Rajtar B, Bachanek T, Piątek D, Bugla-Płoskońska G, Lukowiak A (2021) Composite based on graphite oxide, metallic silver and zirconium phthalocyanine coordinated by out-of-plane argininate ligands as photoactive antibacterial additive to endodontic cement. J Photochem Photobiol A 418:113432. https://doi.org/10.1016/j.jphotochem.2021.113432
36. Min Y, Zhang K, Zhao W, Zheng F, Chen Y, Zhang Y (2012) Enhanced chemical interaction between TiO_2 and graphene oxide for photocatalytic decolorization of methylene blue. Chem Eng J 203:193. https://doi.org/10.1016/j.cej.2012.04.047
37. Montes-Navajas P, Asenjo NG, Santamaría R, Menéndez R, Corma A, García H (2013) Surface area measurement of graphene oxide in aqueous solutions. Langmuir 29:13443. https://doi.org/10.1021/la4029904
38. Elkin I. (2009) The influence of low-pressure cold plasma on biological activity of immunocytes. Preliminary report. Acta Bio-Optica et Informatica Medica. Inżynieria Biomedyczna 15(4):397.
39. Psuja P, Strek W, Yelkin I (2014) Non-thermal plasma-driven synthesis of Eu^{3+}:Y_2O_3 nanosized phosphors. J Nanopart Res 16(1):2176. https://doi.org/10.1007/s11051-013-2176-2
40. Milburn TR, Beadle LC (1960) The determination of total Carbon dioxide in water. J Exp Biol 37:444
41. Thema FT, Moloto MJ, Dikio ED, Nyangiwe NN, Kotsedi L, Maaza M, Khenfouch M (2013) Synthesis and characterization of graphene thin films by chemical reduction of exfoliated and intercalated graphite oxide. J Chem 2013:150536. https://doi.org/10.1155/2013/150536
42. Li G, Wu J, Jin H, Xia Y, Liu J, He Q, Chen D (2020) Titania/Electro-Reduced Graphene Oxide Nanohybrid as an Efficient Electrochemical Sensor for the Determination of Allura Red. Nanomaterials 10(2):307. https://doi.org/10.3390/nano10020307
43. Pan N, Guan D, He T, Wang R, Wyman I, Jin Y, Xia C (2013) Removal of Th^{4+} ions from aqueous solutions by graphene oxide. J Radioanal Nucl Chem 298:1999. https://doi.org/10.1007/s10967-013-2660-2
44. Praveen P, Viruthagiri G, Mugundan S, Shanmugam N (2014) Structural, optical and morphological analyses of pristine titanium di-oxide nanoparticles – Synthesized via sol–gel route. Spectrochimica Acta A 117:622. https://doi.org/10.1016/j.saa.2013.09.037
45. Štengl V, Bakardjieva S, Grygar TM, Bludská J, Kormunda M (2013) TiO2-graphene oxide nanocomposite as advanced photocatalytic materials. Chem Cent J 7:41. https://doi.org/10.1186/1752-153X-7-41
46. Khan F, Khan MS, Kamal S, Arshad M, Ahmad SI, Nami SAA (2020) Recent advances in graphene oxide and reduced graphene oxide based nanocomposites for the photodegradation of dyes. J Mater Chem C 8:15940. https://doi.org/10.1039/D0TC03684F
47. Liua R, Li X, Li S, Zhou G (2017) Three-dimensional titanate–Graphene oxide composite gel with enhanced photocatalytic activity synthesized from nanofiber networks, Catal Today 297:264; https://doi.org/10.1016/j.cattod.2016.12.046
48. Chia CH, Razali NF, Sajab MS, Zakaria S, Huang NM, Lim HN (2013) Methylene blue adsorption on graphene oxide. Sains Malaysiana 42(6):819
49. Yang H, Zhai L, Li K, Liu X, Deng B, Xu W (2020) A highly efficient nano-graphite-doped TiO2 photocatalyst with a unique sea-island structure for visible-light degradation. Catal Sci Technol 10:1161. https://doi.org/10.1039/C9CY02179E
50. Gohari-Bajestani Z, Akhlaghi O, Yürüm Y, Yürüm A (2017) Synthesis of anatase TiO2 with exposed (001) facets grown on N-doped reduced graphene oxide for enhanced hydrogen storage. Int J Hydrogen Energy 42(9):6096. https://doi.org/10.1016/j.ijhydene.2016.11.069